Progress In Electromagnetics Research, Vol. 134, 247–266, 2013

ISOLATION IMPROVEMENT IN A DUAL-BAND DUAL-ELEMENT MIMO ANTENNA SYSTEM USING CAPACITIVELY LOADED LOOPS

Mohammad S. Sharawi[1, *], Ahmed B. Numan[1], and Daniel N. Aloi[2]

[1]Electrical Engineering Department, King Fahd University for Petroleum and Minerals (KFUPM), Dhahran 31261, Saudi Arabia

[2]Electrical and Computer Engineering Department, Oakland University, Rochester, Michigan 48309, USA

Abstract—A dual-band dual-element multiple-input-multiple-output (MIMO) antenna system with enhanced isolation is proposed. The MIMO antenna system is based on printed 4-shaped antenna elements. Dual band isolation is achieved by using an array of printed capacitively loaded loops (CLLs) on the top side of the board for high band isolation improvement and a complementary CLL structure on the GND plane of the antenna for lower band isolation improvement. The lower band of operation covers 827–853 MHz and the higher band covers 2.3–2.98 GHz. Two prototypes were investigated to access the effect of the isolation mechanism. Measured isolation improvement of 10 dB was observed in the lower operating band while the improvement in the higher band was approximately 2.5 dB. The isolation improvement was at the expense of 5% reduction in efficiency. The measured gain patterns as well MIMO figures of merits such as the correlation factor, TARC and MEG were investigated as well.

1. INTRODUCTION

Fourth generation wireless systems (also called Long Term Evolution — LTE) rely on the use of multiple-input-multiple-output (MIMO) antenna systems integrated within the user terminals in order to achieve higher data rates and multimedia capabilities. This poses a challenge in terms of the antenna size and the achievable isolation

Received 6 September 2012, Accepted 6 November 2012, Scheduled 24 November 2012

* Corresponding author: Mohammad S. Sharawi (msharawi@kfupm.edu.sa).

between adjacent radiating elements that affects the overall diversity performance of the system [1–3].

Improving the isolation between adjacent MIMO antennas is a challenging task especially for technologies that operate at low frequency bands (Low frequency LTE bands). There are a number of techniques that are used to enhance the isolation between the antennas. Reported techniques in literature include the introduction of the decoupling structures [4], modifications in the ground plane [5–7], lumped component filters [8], neutralization strips [9–11], introduction of resonating structures near the antennas [12], antenna orientation [13] and the use of metamaterials [14–16].

Metamaterials are artificially engineered materials that possess properties not found in nature (i.e., negative permittivity or permeability). These materials are usually realized by periodically repeating a basic unit element (UE) structure. Metamaterials can exhibit stop band filter properties [17]. This property is used to isolate closely packed antennas. Thus, the metamaterial should be designed properly to have a stop band at the desired frequency.

Capacitively loaded loops (CLLs) were introduced in [18–20]. They were modeled in [21] using method of moment (MoM) and an interpolation scheme. The resonance frequency is determined by the configuration and physical dimensions of the loop. A metamaterial can be realized by periodically placing copies of the UE (i.e., the CLL). The dimensions of CLL determine the band in which the material will have metamaterial properties.

In [14], a MIMO antenna system consisting of two monopole antennas separated by 0.18 wavelengths operating at 2.6 GHz for WiMAX applications was proposed. The metamaterial between the antennas is formed using two different configurations of CLLs. 6 dB isolation improvement was obtained. In [15], non-planar split ring resonators (SRRs) were used to enhance the isolation between two radiating elements (monopoles) operating in the 3.38–3.7 GHz frequency band. The maximum isolation within the desired band was improved by about 3 dB. In [16], a metamaterial based channel isolator was introduced to enhance the isolation between two printed spiral MIMO antennas operating in the commercial ISM band around 2.5 GHz. This isolation method realizes an artificial magnetic wall that decouples the radiating elements from coupling through the magnetic field. The magnetic wall improved the isolation by 24 dB. This method is only applicable for spiral antenna types.

Almost all the work that appeared in literature to enhance the isolation between adjacent MIMO antennas focused on high frequency bands (above 1 GHz) as size of UE increases as the frequency of

operation decreases. Large size UE violate the strict constraints on the area of a printed MIMO antenna system especially for handheld devices. This work focuses on improving the isolation between adjacent MIMO antenna elements operating in the sub-GHz frequencies using spiral-like CLLs. The CLL selected has the tendency of having higher values of capacitance and inductance in a limited area by varying the parameters of the spirals associated with the UE and hence the stop band can be achieved at low frequencies. In addition to the lower frequency metamaterial design, this work proposes a metamaterial configuration that covers the higher band of operation as well, thus the complete structure is suitable for enhancing the isolation of dual-band MIMO antenna systems.

The 4-shaped MIMO antenna system with its novel antenna element geometry first appeared in [22] and [23]. This antenna is a dual band one and its measured isolation in the low band was very poor. The proposed isolation mechanism for dual band isolation enhancement using spiral like CLL arrays is applied to the dual band 4-shaped MIMO antenna system. The simulated and measured MIMO antenna performance metrics such as the *s*-parameters, gain patterns, total active reflection coefficient (TARC) as well as the mean effective gain (MEG) are presented and discussed. An isolation improvement of 10 dB in the low band and 2.5 dB in the high band are observed with this new isolation mechanism. This of course came as a trade off with lowering the efficiency of the MIMO antenna system by approximately 5%.

The rest of the paper is organized as follows: Section 2 describes the modeling of the dual band 2×1 MIMO antenna system with the proposed CLL isolation arrays. Section 3 presents and compares the simulation and measurement results and Section 4 concludes the paper.

2. THE 2×1 MIMO ANTENNA DESIGN WITH CLLs

The original 2×1 MIMO antenna system of 4-shaped elements is shown in Figure 1. Please note that the top layer has the antennas while the bottom layer has the ground plane. This model is called Model A from now on. The basic antenna element has the shape of the number 4, and hence it is called the 4-shaped antenna. The modified MIMO antenna system with the added capacitively loaded loops (CLLs) on the top side and etched out from the GND plane at the bottom side is shown in Figure 2. This antenna model is called Model B from now on. The antennas were designed and optimized using the field solver HFSS^{TM}.

The dimensions of the 2×1 dual band MIMO antenna Model A were (in mm): $W = 50$, $L = 100$, $W_t = 2.2$, $H = 2.5493$, $L_1 = 40.75$,

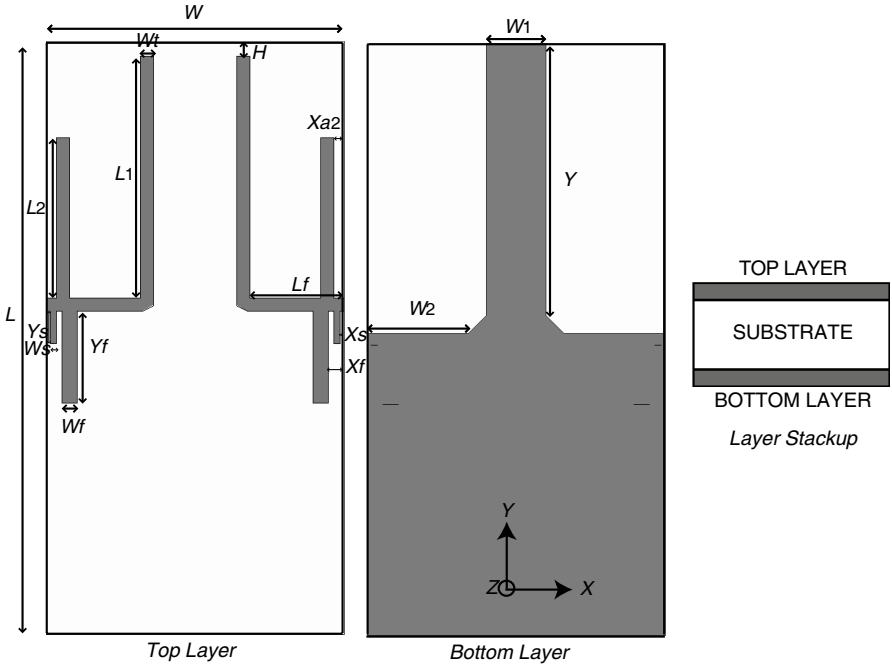

Figure 1. Geometry of the 2×1 4-shaped MIMO antenna system Model A.

$L_2 = 27$, $Y_s = 5.5$, $X_{a2} = 1.6716$, $L_f = 15.8$, $X_s = 0.6716$, $X_f = 2.6716$, $W_f = 2.5$, $W_s = 1$, $Y_f = 15.5$, $W_1 = 10$, $Y = 46$ and $W_2 = 17$. The antenna was printed on an FR-4 substrate of thickness 1.56 mm, 1 oz. copper plating and a dielectric constant of 4.4. The overall size of the two-element dual band MIMO antenna system was $50 \times 100 \times 1.56\,\text{mm}^3$.

The top side CLLs were designed to operate at 2.75 GHz, because it is the the resonance frequency of the 4-shaped antenna at the high band before applying the CLLs. The resonance frequency of the metamaterial unit element (UE) (or unit cell) depends on the inductance and capacitance of the structure. The gap between the spiral traces need to be increased in order to lower these values. Similarly the number of edges of the spirals associated with UEs should also be reduced along with the reduction of the size of unit cell. This reduces the length of coupled edges which results in a reduction of the capacitance and inductance associated with the UE structure. Thus, a small UE with a higher gap and small number of the spiral edges resonates at higher frequencies. An array of UE was deployed between

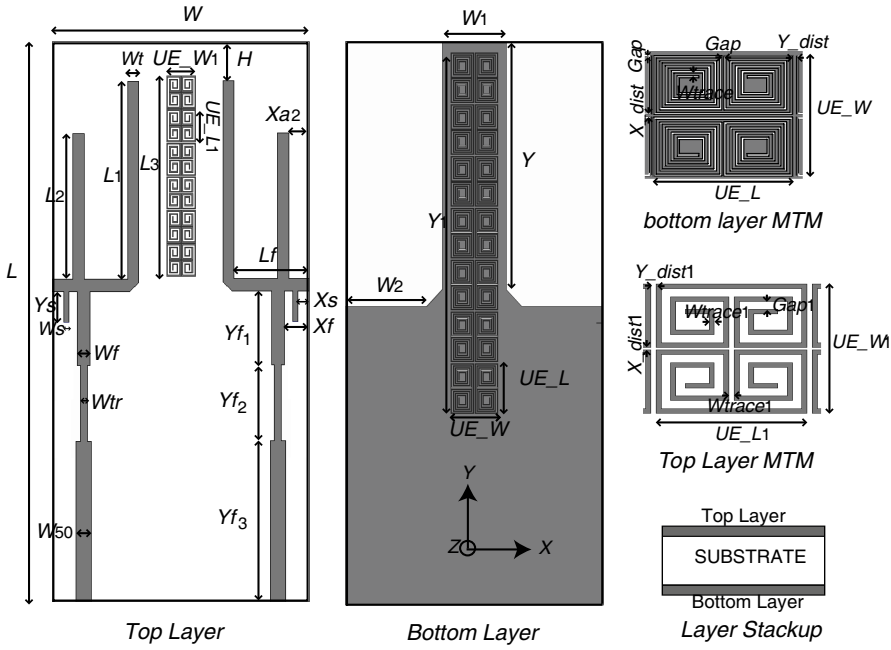

Figure 2. Geometry of the 2×1 4-shaped MIMO antenna system Model B.

the antennas on the top layer for high frequency isolation enhancement. The UE size was $5.727 \times 5.8\,\text{mm}^2$, with a line width of 0.2 mm and inter-element spacing of 0.127 mm in the x-direction and 0.2 mm in the y-direction. A larger sized UE for the lower band operation was designed by increasing the number of loops within the spiral and tuning the other parameters to have it resonate around 800 MHz. This CLL was etched out from the GND plane (complementary CLL) and had dimensions of $9 \times 8.927\,\text{mm}^2$ with inter-element separation of 0.2 mm in the x-direction and 0.273 mm in the y-direction. The trace width (etched out from GND plane) was 0.25 mm.

Figure 3 shows the dispersion diagrams for lower and higher band CLL arrays. In Figure 3(a), the high frequency dispersion curves for the first two modes are shown. The band gap between the two modes is evident between 1.75 GHz and 2.22 GHz. Figure 3(b) shows the lower band dispersion curves for the first two modes. The band gap between the two modes is clear between 750 MHz and 842 MHz. It is worth noting that these diagrams are based on an infinite periodic arrangement of the UE within the modeling tool. Figure 4 shows the transmission coefficient taken when a simple microstrip transmission

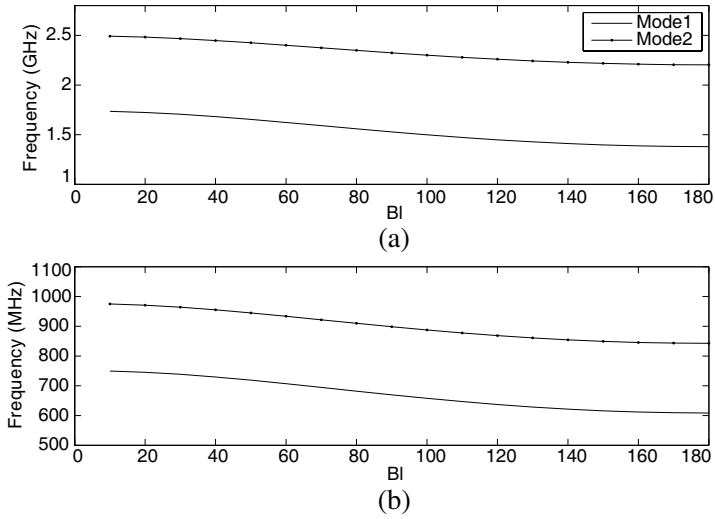

Figure 3. Dispersion curves for the (a) high and (b) low band CLL arrays.

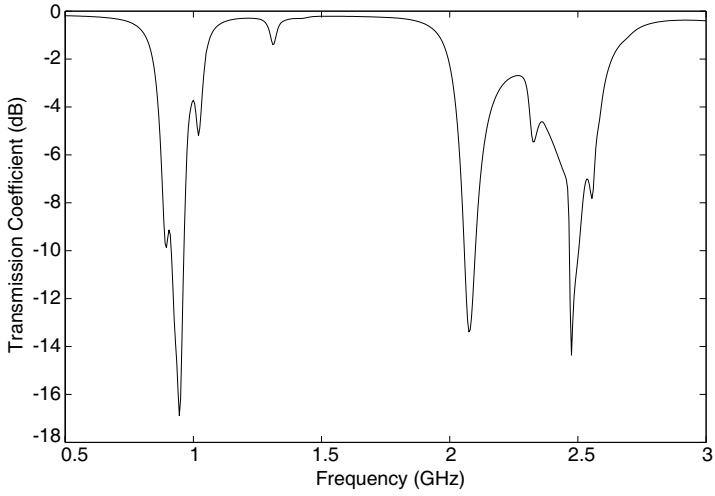

Figure 4. Transmission coefficient of the proposed printed CLL arrays.

line is passed over the top and bottom CLL arrays. An extra layer of 0.07 mm thickness was added for the microstrip line to test the transmission coefficient. The isolation in the lower band centered at

940 MHz and higher bands at 2 GHz and 2.5 GHz are clear. These values were tuned to operate within the bands of interest when the CLL arrays were applied between the antennas.

The dimensions of Model B were (in mm): $W = 50$, $L = 100$, $W_t = 2.2$, $H = 6.9635$, $L_1 = 35.3$, $L_2 = 26$, $Y_s = 5.5$, $X_{a2} = 4.0716$, $L_f = 14.7$, $X_s = 0.3716$, $X_f = 1.5716$, $W_f = 2.5$, $W_s = 1$, $W_{tr} = 1.4$, $W_{50} = 3$, $Y_{f1} = 13.35$, $Y_{f2} = 13.5$, $Y_{f3} = 28.65$, $UE\_W_1 = 5.727$, $UE\_L_1 = 5.8$, $L_3 = 35.8$, $W_1 = 12.2$, $UE\_W = 9$, $UE\_L = 8.927$, $Y_1 = 64.127$, $Y = 44$, $W_2 = 15.9$, $Y\_dist = 0.273$, $Gap = 0.127$, $X\_dist = 0.2$, $W_{trace=}0.25$, $Y\_dist1 = 0.2$, $X\_dist1 = 0.127$, $GAP_1 = 0.36$, $W_{trace1} = 0.2$.

3. RESULTS AND DISCUSSION

Figure 5 shows the fabricated antenna structure of Model A (Top and Bottom views) while Figure 6 shows the fabricated MIMO antenna Model B. The S-parameter measurements for these 2×1 4-shaped MIMO antenna system are shown in Figure 7 for the low and high bands of operation for Model A, and in Figure 8 for the low and high bands of operation of Model B. A 50 Ω termination was used on the other port during the S_{ii} measurement, where $i \in [1, 2]$. Figure 7(a) shows the measured and simulated S-parameter curves for the lower band for antenna elements 1 and 2 covering the 762–790 MHz. A

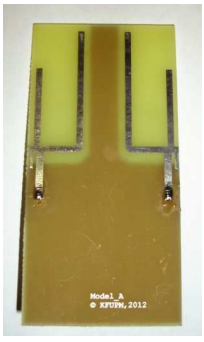

(a) (b)

Figure 5. Fabricated dual-band 4-shaped MIMO antenna system Model A. (a) Top side. (b) Bottom side.

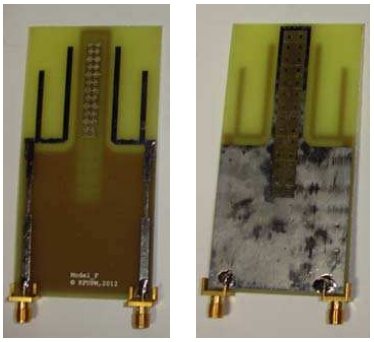

(a) (b)

Figure 6. Fabricated dual-band 4-shaped MIMO antenna system Model B. (a) Top side. (b) Bottom side.

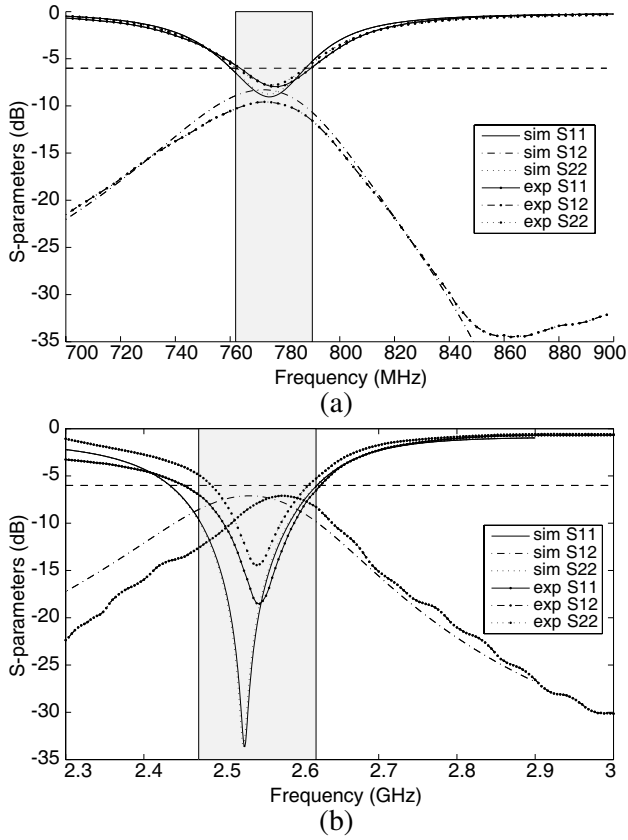

Figure 7. S-parameter measurements of the fabricated 2×1 4-shaped MIMO antenna Model A. (a) Lower band. (b) Upper band.

-6 dB bandwidth (BW) of 28 MHz was obtained[†]. Figure 7(b) shows the measured and simulated S-parameter curves for the upper band for elements 1 and 2 covering 2.45–2.625 GHz and 2.485–2.61 GHz, respectively. A -6 dB BW of more than 125 MHz was obtained. The discrepancies between the measured and simulated curves are due the fabrication process. The minimum measured isolation in the lower band was approximately 9.5 dB while in the upper band it was approximately 7.1 dB.

The results for Model B are shown in Figure 8. Figure 8(a) shows the lower band S-parameter measurements, while Figure 8(b) shows the higher band ones. The lower band covered the frequency ranges

[†] The -6 dB BW is widely accepted for evaluating closely packed MIMO antenna systems such as in [24–27].

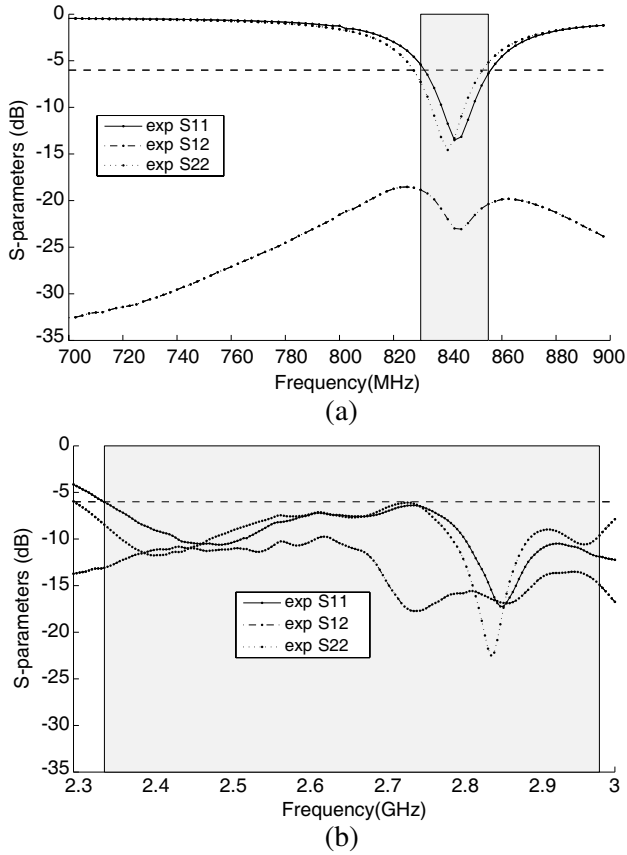

Figure 8. S-parameter measurements of the fabricated 2×1 4-shaped MIMO antenna Model B. (a) Lower band, (b) Upper band.

from 827–853 MHz and 831–856 MHz for elements 1 and 2, respectively. A minimum −6 dB BW of 26 MHz was measured. The higher band covered from 2.3–2.98 GHz for both elements 1 and 2. The measured −6 dB BW was 640 MHz. The minimum measured isolation in the lower band was improved by about 10 dB to reach 18.9 dB after the introduction of CLLs in the top and bottom layers. The minimum measured isolation in higher band of operation was improved by approximately 2.5 dB to reach 9.8 dB. Note that the spatial separation at the lower band (800 MHz) is less than $\lambda_0/15$, which justifies the use of CLLs to improved the isolation. Although the addition of CLL arrays improved the isolation in both bands, it shifted the resonance frequency of the lower band upwards by approximately 65 MHz. It also widened the upper band BW.

The original impedance of Model B was not 50 Ω. This means that the antenna response varies as we change the length of the feed line. An impedance transformer is introduced to match the antenna impedance. The impedance transformer should be capable of providing acceptable match at both bands. The low band impedance is matched via tuning the antenna structure and we used a $\lambda/4$ microstrip impedance transformer for the high band matching. After tuning the antenna without the introduction of the impedance transformer, the input impedance becomes $(48.32 + j2.6)\,\Omega$ at 840 MHz and $(117.3 + j0.61)\,\Omega$ at 2.75 GHz. After placing and tuning the microstrip impedance transformer (length = 13.5 mm, width = 1.4 mm), we obtain $(42.4 - j0.36)\,\Omega$ at 840 MHz and $(57.7 - j6.03)\,\Omega$ at 2.85 GHz. So the impedance is almost matched to 50 Ω. The impedance at the low band is not much affected by the microstrip impedance transformer. The feeding positions of Models A and B were located at the points of 50 Ω matching. The impedance transformer was optimized to give good input matching while maintaining the maximum isolation levels.

The effect of the CLL arrays on the current distribution on the antenna elements and the GND plane are shown for the two bands and two antenna models in Figure 9. Figures 9(a) and (b) compare side by side the current distributions of Models A and B in the lower band of operation, while Figures 9(c) and (d) compare side by side the current distributions of Models A and B in the higher band of operation. It is clear that the introduction of the CLLs on the top and bottom layers of the antenna had a major influence on the current distribution that in effect enhanced the coupling between the two closely packed antenna elements in both the lower and higher bands of operation.

The measured gain patterns of the proposed MIMO antenna system were obtained using an outdoor antenna range facility at Oakland University, Michigan, USA. Figure 10 shows the measured normalized radiation gain patterns of the MIMO antenna system proposed at 775 MHz and 2550 MHz bands for Model A. The 775 MHz x-z plane (elevation plane with $\phi = 0°$) is shown in Figure 10(a) while the y-z (elevation plane with $\phi = 90°$) plane is shown in Figure 10(b). In both figures, the co-pol and cross-pol patterns for antenna elements 1 and 2 are shown. The maximum measured gain at 775 MHz was −4 dBi. Similarly, the x-z and y-z plane cut gain patterns for antenna elements 1 and 2 at 2550 MHz are shown in Figures 10(c) and (d), respectively. The maximum measured gain at the high band was 2.5 dBi. The low band efficiency was $\eta_{low} = 40\%$ while the high band one was $\eta_{high} = 75\%$.

The measured normalized gain patterns of Model B are shown in Figure 11 for the low and high bands of operation. The 840 MHz x-z

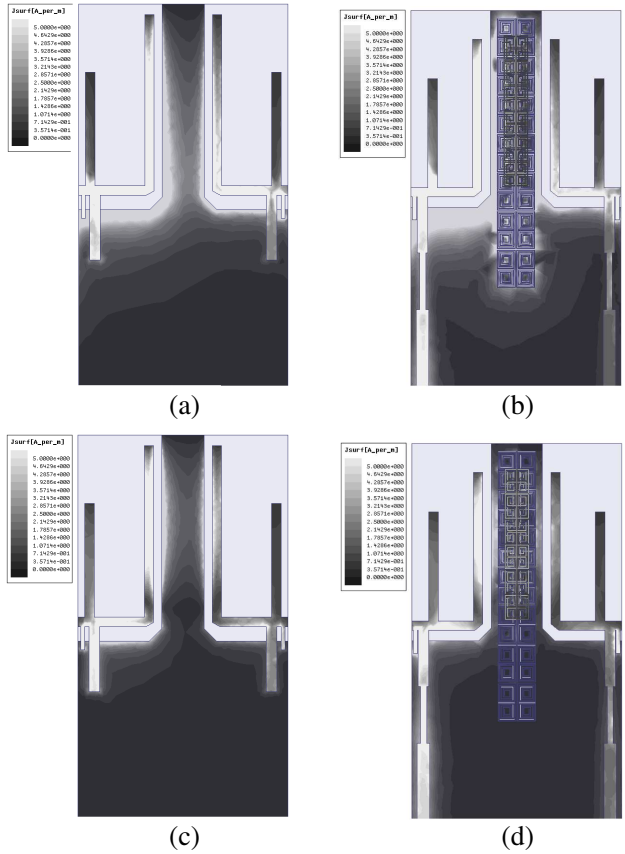

Figure 9. Current distribution plots. (a) Model A at 755 MHz. (b) Model B at 840 MHz. (c) Model A at 2550 MHz. (d) Model B at 2850 MHz.

plane (elevation plane with $\phi = 0°$) is shown in Figure 11(a) while the y-z (elevation plane with $\phi = 90°$) plane is shown in Figure 11(b). In both figures, the co-pol and cross-pol patterns for antenna elements 1 and 2 are shown. The maximum measured gain at 840 MHz was -2.8 dBi. Similarly, the x-z and y-z plane cut gain patterns for antenna elements 1 and 2 at 2850 MHz are shown in Figures 11(c) and (d), respectively. The maximum measured gain at the high band was 5.5 dBi. The low band efficiency was $\eta_{low} = 35\%$ while the high band one was $\eta_{high} = 67\%$. The introduction of the MTM lowered the efficiency of the antenna at both bands, introduced several dips in the gain pattern and increased its directivity. The discrepancies between

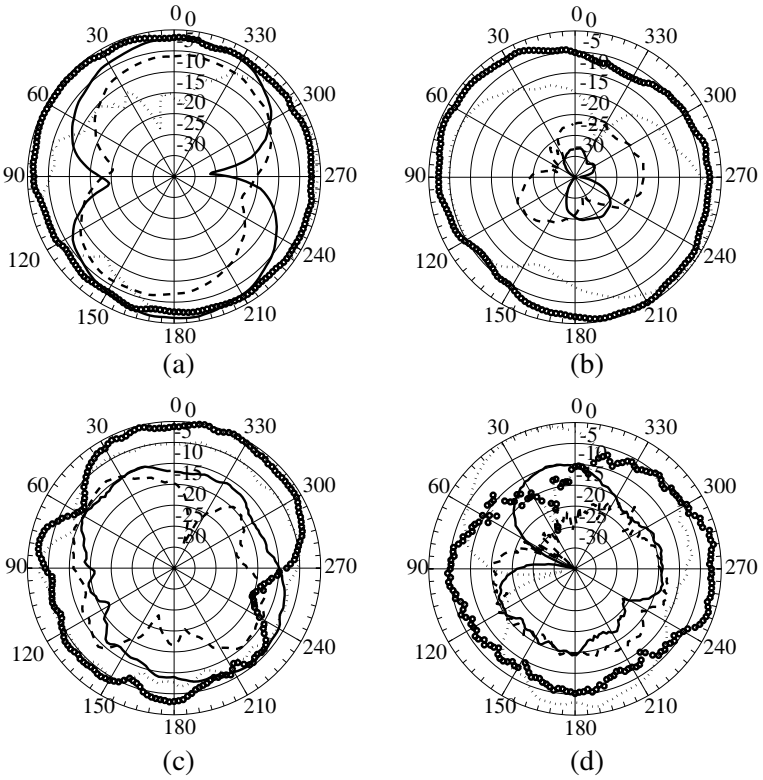

Figure 10. Measured gain patterns for the proposed MIMO antenna Model A. (a) x-z plane at 755 MHz. (b) y-z plane at 755 MHz. (c) x-z plane at 2550 MHz. (d) y-z plane at 2550 MHz. Dots is co-pol element 1, Circles is co-pol element 2, solid is cross-pol element 1, dashes is cross-pol element 2.

some of the patterns of elements 1 and 2 are believed to be due to the measurement setup and antenna mounting on the plastic stand. The pattern dip occurring might be due to placing it close to the stand edge or because of placing some tape on top of it. The relatively low efficiency at the lower band of operation is attributed to the fact that the basic antenna element (4-shaped antenna) is an electrically small one. And thus, adding the CLLs as isolation enhancement elements only degraded the efficiency by 5%. This is a tradeoff that the designer should be aware of when using ESA as well as MTM based structures as was also indicated in [28, 29].

The MIMO antenna system correlation factor will be significantly degraded with higher coupling levels. It can be calculated from

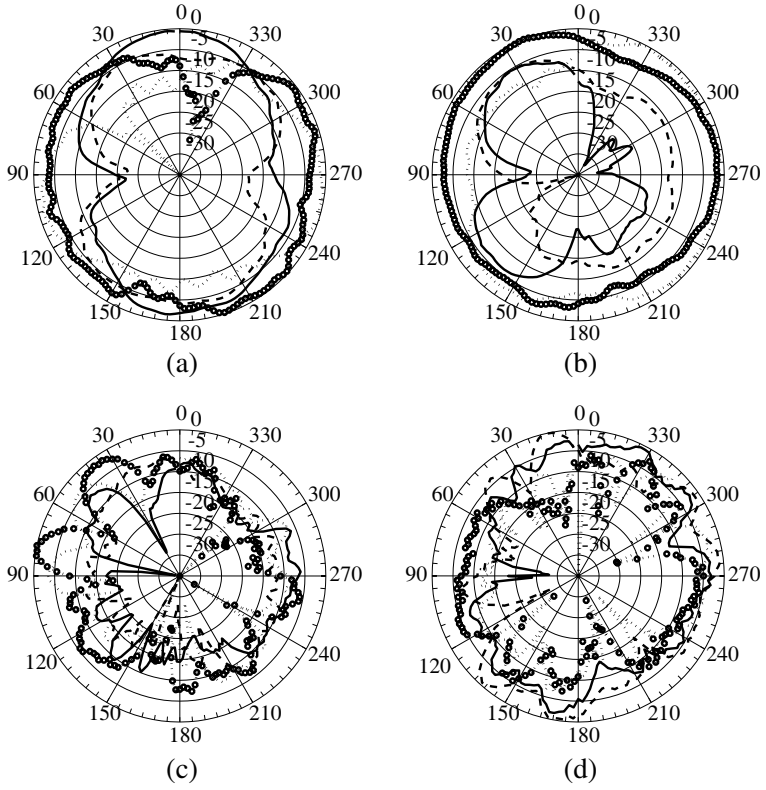

Figure 11. Measured Gain patterns for the proposed MIMO antenna Model B. (a) x-z plane at 840 MHz. (b) y-z plane at 840 MHz. (c) x-z plane at 2850 MHz. (d) y-z plane at 2850 MHz. Dots is co-pol element 1, Circles is co-pol element 2, solid is cross-pol element 1, dashes is cross-pol element 2.

the measured s-parameters in isotropic/uniform signal propagation environments [30]. The correlation factor (ρ) is important to achieve the required diversity gain of the MIMO antenna system. The lower the ρ value, the higher the diversity gain. The antenna efficiency is also another factor needed for determining the correlation factor. The value of ρ can be calculated using:

$$|\rho_{ij}| = \frac{|S_{ii}^* S_{ij} + S_{ij}^* S_{jj}|}{\sqrt{|(1 - |S_{ii}^2| - |S_{ji}^2|)(1 - |S_{jj}^2| - |S_{ij}^2|)\eta_i \eta_j|}} \tag{1}$$

Even with the presence of the relatively low isolation values specially in the higher band (approximately 10 dB), the calculated

values of the correlation factor for Model B at the the lower and higher bands of operation were less than 0.11 and 0.18, respectively. Figure 12 shows the lower band and higher band correlation factor curves for Model B. It is evident that this MIMO antenna system with enhanced isolation will satisfy the LTE requirements for spatial diversity since the values of $|\rho| \leq 0.3$ for the bands of interest [2].

The total active reflection coefficient (TARC) is considered the MIMO array radiation efficiency for multi-ports antennas [31]. It is calculated by finding the ratio between the square root of the total reflected power divided by the square root of the total incident power,

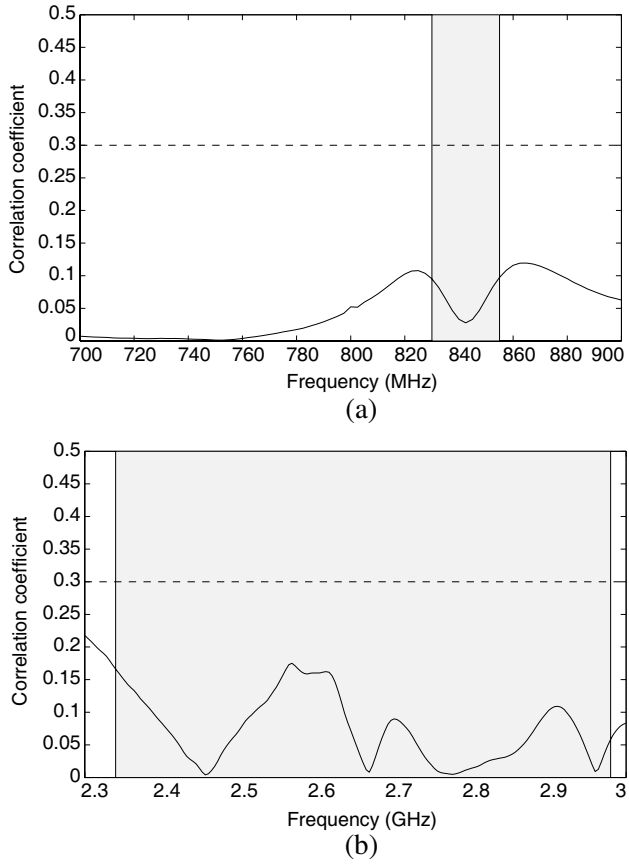

Figure 12. Correlation factor $|\rho_{12}|$ curves for Model B. (a) Lower band, (b) higher band of operation.

it is found using:

$$\Gamma = \frac{\sqrt{|(S_{11} + S_{12}e^{j\theta})|^2 + |(S_{21} + S_{22}e^{j\theta})|^2}}{\sqrt{2}} \tag{2}$$

where θ is the phase angle between the two ports. Figure 13 shows the TARC curves for the low band and high band of operation for Model B. The phase differences were swept between 0 and 180 degrees in 30 degree steps. It is evident that the TARC for the low band is almost always less than -6 dB, while in the high band, it goes up to -4 dB. TARC values become worse when 180° phase difference between the two port waves is considered (when out of phase incident signals on element 2 with respect to element 1). Such levels have also been reported to give good diversity gain as indicated in [32].

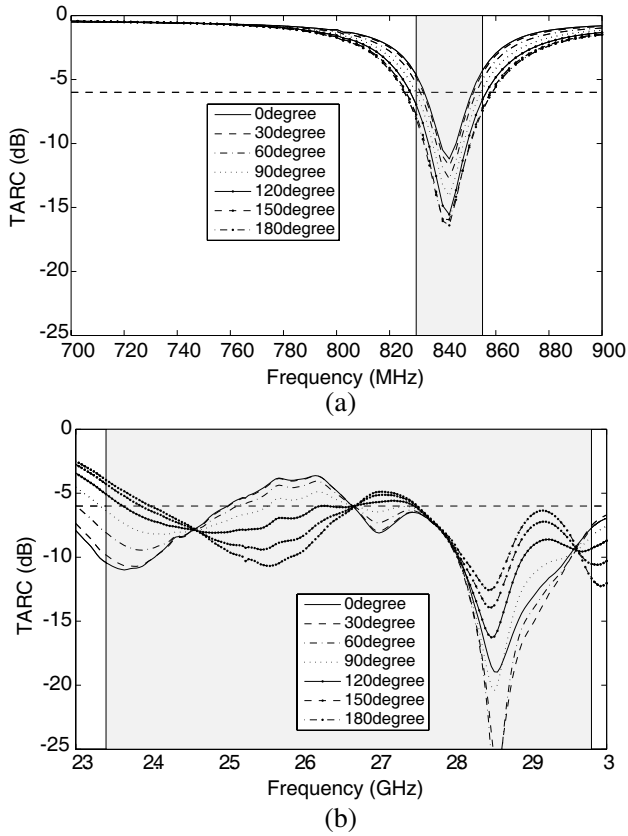

Figure 13. TARC curves for Model B. (a) Lower band, (b) higher band of operation.

In addition to ρ and TARC, the mean effective gain (MEG) is another parameter that directly affect the diversity gain and performance of a MIMO antenna system. MEG can be calculated by finding the ratio of the mean received power to the mean incident power of the antenna. This is found using [33]:

$$\text{MEG} = \oint \left[\frac{\text{XPD}}{1+\text{XPD}} p_\theta(\Omega) G_\theta(\Omega) + \frac{1}{1+\text{XPD}} p_\phi(\Omega) G_\phi(\Omega) \right] d\Omega \quad (3)$$

where XPD is the cross-polarization discrimination of the incident field (ratio between the vertical and horizontal power densities), p_θ and p_ϕ are the θ and ϕ components of the probability distribution functions of the incoming wave, respectively. G_θ and G_ϕ are the power gain patterns of the antenna. Following the same mobile communications channel assumptions as in [34] MEG can be evaluated using,

$$\text{MEG} = \frac{1}{2\pi} \int_0^{2\pi} \left[\frac{\text{XPD}}{1+\text{XPD}} G_\theta\left(\frac{\pi}{2}, \phi\right) + \frac{1}{1+\text{XPD}} G_\phi\left(\frac{\pi}{2}, \phi\right) \right] d\phi \quad (4)$$

The calculated MEG values for the proposed antenna system for the low bands and high bands with cross-polarization discrimination (XPD-Γ) of 0 dB and 6 dB are presented in Table 1 for both Models A and B. It is evident that the ratio of $\text{MEG}_1/\text{MEG}_2 < 3$ dB at both bands of operation with both XPD values. This will provide acceptable diversity gain as indicated in [33]. In addition, Table 1 shows the minimum isolation levels, minimum efficiencies and maximum correlation coefficient values in the band of operation of the models proposed.

Table 1.

Frequency (MHz)	Min. Isolation (dB)	Min. η (%)	$\lvert\rho_{12}\rvert$	MEG_1 (XPD = 0 dB)	MEG_2 (XPD = 0 dB)	MEG_1 (XPD = 6 dB)	MEG_2 (XPD = 6 dB)
755 (Model-A)	9.5	40	0.4	−10.0	−9.98	−13.83	−13.83
2550 (Model-A)	7.1	75	0.15	−2.94	−2.97	−6.73	−6.75
840 (Model-B)	18.9	35	0.11	−10.15	−10.16	−13.94	−13.94
2850 (Model-B)	9.8	67	0.18	−3.2	−3.24	−7.13	−7.1

4. CONCLUSIONS

The design and fabrication of two dual-element dual-band MIMO antenna systems based on 4-shaped printed antenna structures was represented. An isolation enhancement method for the dual bands was introduced and investigated. The isolation method was based on using arrays of CLLs on the top layer of the PCB while complementary CLLs were used on the bottom layer of the board. The MIMO antenna system covers 827–853 MHz and 2.3–2.98 GHz. The isolation improvement was more than 10 dB in the lower band and 2.5 dB in the higher band. Measured antenna gain patterns were presented. A maximum gain of 5.5 dB was obtained in the higher band while −2.8 dB was obtained in the lower band. The correlation factor, TARC and MEG values of this MIMO antenna system were also calculated and shown to provide good diversity performance.

ACKNOWLEDGMENT

This work was supported by project number RG1219 through the Deanship of Scientific Research at KFUPM, Dhahran, Saudi Arabia.

REFERENCES

1. Song, L. and J. Shen, *Evolved Cellular Network Planning and Optimization for UMTS and LTE*, CRC Press, 2011.
2. 3GPP TS 36.101, V8.3.0, "EUTRA User Equipment Radio Transmission and Reception," September 2008.
3. Gesbert, D., S. Mansoor, S. Da-shan, P. J. Smith, and A. Naguib, "From theory to practice: An overview of MIMO space-time coded wireless systems," *IEEE J. Sel. Areas Commun.*, Vol. 21, No. 3, 281–302, Apr. 2003.
4. Yoo, S. and S. Kahng, "A compact MIMO antenna using ZOR split ring resonator radiators with a decoupling structure," *Microwave Journal*, Vol. 54, No. 11, S26–S31, November 2011.
5. Li, H., J. Xiong, Z. Ying, and S. He, "High isolation compact four-port MIMO antenna systems with built-in filters as isolation structure," *Proceedings of the Fourth European Conference on Antennas and Propagation (EuCAP)*, 1–4, 2010.
6. Chou, H. T., H. C. Cheng, H. T. Hsu, and L. R. Kuo, "Investigations of isolation improvement techniques for Multiple Input Multiple Output (MIMO) WLAN portable terminal

applications," *Progress In Electromagnetics Research*, Vol. 85, 349–366, 2008.

7. Zhu, F., J. Xu, and Q. Xu, "Reduction of mutual coupling between closely-packed antenna elements using defected ground structure," *Electronics Letters*, Vol. 45, No. 12, 601–602, 2009.
8. Han, M. and J. Choi, "Multiband MIMO antenna with a band stop filter for high isolation characteristics," *Antennas and Propagation Society International Symposium*, 1–4, 2009.
9. Yeom, I., J. Kim, and C. Jung, "Compact dual-band MIMO antenna with high isolation performance," *Asia-Pacific Microwave Conference Proceedings (APMC)*, 766–769, 2010.
10. Li, Z., M. Han, X. Zhao, and J. Choi, "MIMO antenna with isolation enhancement for wireless USB dongle application at WLAN band," *Antennas and Propagation Society International Symposium*, 758–761, 2010.
11. Lee, C., S. Chen, and P. Hsu, "Integrated dual planar inverted-F antenna with enhanced isolation," *IEEE Antennas and Wireless Propagation Letters*, Vol. 8, 963–965, 2009.
12. Min, K., D. Kim, and Y. Moon, "Improved MIMO antenna by mutual coupling suppression between elements," *The European Conference on Wireless Technology*, 125–128, 2005.
13. Karaboikis, M., C. Soras, G. Tsachtsiris, and V. Makios, "Compact dual-printed inverted-F antenna diversity systems for portable wireless devices," *IEEE Antennas and Wireless Propagation Letters*, Vol. 3, No. 1, 9–14, 2004.
14. Hsu, C., K. Lin, H. Su, H. Lin, and C. Wu, "Design of MIMO antennas with strong isolation for portable applications," *IEEE Antennas and Propagation Society International Symposium*, 1–4, 2009.
15. Lee, Y., H. Chung, J. Ha, and L. Choi, "Design of a MIMO antenna with improved isolation using meta-material," *International Workshop on Antenna Technology (iWAT'11)*, 231–234, 2011.
16. Sarabandi, K. and Y. J. Song, "Subwavelength radio repeater system utilizing miniaturized antennas and metamaterial channel isolator," *IEEE Transactions on Antennas and Propagation*, Vol. 59, No. 7, 2683–2690, 2011.
17. Marques, R., F. Martin, and M. Sorolla, *Metamaterials with Negative Parameters: Theory, Design and Microwave Applications*, John Wiley and Sons, 2011.
18. Guo, Y. and R. Xu, "Planar metamaterials supporting multiple

left-handed modes," *Progress In Electromagnetics Research*, Vol. 66, 239–251, 2006.

19. Hrabar, S., Z. Eres, and J. Bartolic, "Capacitively loaded loop as basic element of negative permeability meta-material," *32nd European Microwave Conference*, 1–4, 2002.
20. Goussetis, G., A. P. Feresidis, S. Wang, Y. Guo, and J. C. Vardaxoglou, "Uniplanar left-handed artificial metamaterials," *J. Opt. A: Pure Appl. Opt.*, Vol. 7, No. 2, S44, 2005.
21. Guo, Y., G. Goussetis, A. P. Feresidis, and J. C. Vardaxoglou, "Efficient modeling of novel uniplanar left-handed metamaterials," *IEEE Transactions on Microwave Theory and Techniques*, Vol. 53, No. 4, 1462–1468, 2005.
22. Jan, M. A., D. N. Aloi, and M. S. Sharawi, "A 2×1 compact dual band MIMO antenna system for wireless handheld terminals," *IEEE Radio and Wireless Symposium (RWS 2012)*, Santa Clara, California, January 2012.
23. Sharawi, M. S., M. A. Jan, and D. N. Aloi, "A 4-shaped 2×2 multi-standard compact MIMO antenna system for LTE mobile handsets," *IET Microwaves, Ant. and Prop.*, Vol. 6, No. 6, 685–696, June 2012.
24. Sonkki, M., E. Antonino-Daviu, M. Cabedo-Fabres, M. Ferrando-Bataller, and E. T. Salonen, "Improved planar wideband antenna element and its usage in a mobile MIMO system," *IEEE Antennas and Wireless Propagation Letters*, 1, 2012.
25. Lee, C. J., W. Huang, A. Gummalla, and M. Achour, " Small antennas based on CRLH structures: Concept, design, and applications," *IEEE Antennas and Propagation Magazine,* Vol. 53, No. 2, 10–25, 2011.
26. Han, M.-S. and J. Choi, "MIMO antenna using a decoupling network for next generation mobile application," *9th International Symposium on Communications and Information Technology (ISCIT'09)*, Icheon, South Korea, September 2009.
27. Lopez, N., C. Lee, A. Gummala, and M. Achour, "Compact metamaterial antenna array for Long Term Evolution (LTE) handset application," *IEEE International Workshop on Antenna Techcnology (iWAT'09)*, Santa Monica, California, March 2009.
28. Lee, S. and J. Lee, "Electrically small MNG ZOR antenna with multilayered conductor," *IEEE Antennas and Wireless Propagation Letters*, Vol. 9, 724–727, 2010.
29. Yoo, S. and S. Kahng, "Negative permeability metamaterial structure based electrically small loop antenna," *International*

Conference on Advanced Communication Technology (ICACT), 769–773, 2008.

30. Paul, H., "The significance of radiation efficiencies when using S-parameterss to calculate the received signal correlation from two antennas," *IEEE Antennas and Wireless Propagation Letters*, Vol. 4, No. 1, 97–99, June 2005.
31. Chae, S. H., S. K. Oh, and S. O. Park, "Analysis ofmutual coupling, correlations, and TARC in WiBro MIMO array antenna," *IEEE Antennas and Wireless Propagation Letters*, Vol. 6, 122–125, 2007.
32. Browne, D. W., M. Manteghi, M. P. Fitz, and Y. Rahmat-Samii, "Experiments with compact antenna arrays for MIMO radio communications," *IEEE Transactions on Antennas and Propagation,* Vol. 54, No. 11, 3239–3250, 2006.
33. Ding, Y., Z. Du, K. Gong, and Z. Feng, "A novel dual-band printed diversity antenna for mobile terminals," *IEEE Transactions on Antennas and Propagation*, Vol. 55, No. 7, 2088–2096, July 2007.
34. Ko, S. C. K. and R. D. Murch, "Compact integrated diversity antenna for wireless communications," *IEEE Transactions on Antennas and Propagation*, Vol. 49, 954–960, June 2001.